https://doi.org/10.5194/egusphere-2026-1025
Preprint. Discussion started: 20 April 2026

Contrasting Impacts and Mechanisms of Clustered versus Isolated Summer Atmospheric Rivers on Arctic Sea Ice Melt

Yuzhi Wang[1, *]

[1]College of Atmospheric Sciences, Sun Yat-sen University, Zhuhai, China; wangyzh267@mail2.sysu.edu.cn

Abstract. The rapid decline of Arctic sea ice during summer is increasingly driven by extreme atmospheric moisture transport events, primarily manifested as Atmospheric Rivers (ARs). While the link between individual ARs and localized sea ice loss is well-established, the differential impacts of their temporal distribution—specifically clustered versus isolated occurrences—remain poorly understood. This study investigates the distinct physical mechanisms through which clustered AR sequences and isolated AR events modulate the Arctic surface energy budget and subsequent sea ice retreat.Using high-resolution ERA5 reanalysis data and satellite-derived sea ice concentrations, we identify a paradigm shift in sea ice response depending on AR frequency. Clustered ARs, characterized by successive moisture pulses, induce a "persistent warming effect." This sequence prevents the typical nocturnal radiative cooling and maintains the ice surface skin temperature at the melting point (273.15 K) for extended periods. In contrast, isolated ARs, despite potentially higher peak intensities, often result in transient melting followed by partial thermodynamic recovery. Our analysis reveals that clustered ARs trigger a more potent ice-albedo feedback; the sustained downward longwave radiation (DLR) and latent heat fluxes during clustered events lead to a stepwise reduction in surface albedo that persists long after the moisture pulses subside.Quantitatively, clustered events are associated with a significantly higher number of cumulative melt days and a more profound reduction in net energy gain compared to isolated counterparts of similar total moisture transport volume. These findings suggest that the temporal clustering of ARs is a critical factor in determining the severity of summer sea ice minima, providing a new perspective on the atmospheric driving of the rapidly changing Arctic cryosphere.

1 Introduction

1.1 General Background: The Arctic Climate Crisis and Sea Ice Decline

The Arctic environment is currently undergoing a state of unprecedented transition, exhibiting a rate of surface warming that is nearly four times the global mean—a phenomenon widely recognized as Arctic Amplification. Central to this climatic shift is the dramatic and accelerated reduction of summer sea ice extent, which serves as a critical indicator of the health of the global cryosphere. While the long-term trend of sea ice loss is fundamentally linked to anthropogenic greenhouse gas forcing

https://doi.org/10.5194/egusphere-2026-1025
Preprint. Discussion started: 20 April 2026

(Notz et al., 2020), the interannual variability and extreme minima observed in recent decades are increasingly attributed to synoptic-scale atmospheric processes (Olonscheck et al., 2019). Global climate models (GCMs) within the CMIP6 framework continue to project a transition toward a sea-ice-free Arctic in the coming decades (Guarino et al., 2020; Peng et al., 2020), yet these models often struggle to capture the precise timing and magnitude of abrupt sea ice retreat events triggered by episodic atmospheric forcing.The loss of sea ice is not merely a passive response to rising temperatures but is mediated by complex feedback loops, most notably the ice-albedo feedback. As ice concentration diminishes, the increased exposure of the low-albedo ocean surface enhances solar absorption, further accelerating melt. Recent studies have highlighted that while thermodynamic preconditioning is essential, the "trigger" for the most severe melt seasons often lies in the intrusion of warm and moist air masses from lower latitudes (Mortin et al., 2016).

1.2 The Role of Atmospheric Rivers in Arctic Moisture Transport

In the context of Arctic moisture intrusions, Atmospheric Rivers (ARs) have emerged as the primary conduits for intense poleward water vapor transport (Zhu and Newell, 1998; Guan and Waliser, 2019). Defined as long, narrow filaments of high integrated vapor transport (IVT), ARs are responsible for the vast majority of moisture delivery to the extratropics and polar regions (**?**Nash et al., 2018). These systems are often associated with planetary-scale wave life cycles (Baggett et al., 2016) and the activity of mid-latitude cyclones (Fearon et al., 2021).When ARs penetrate the High Arctic, they induce profound perturbations in the local surface energy budget (Mayer et al., 2019). The arrival of an AR is typically characterized by an abrupt increase in the liquid water path and cloud cover, which dramatically alters the radiative balance. Specifically, the enhanced cloudiness increases the downward longwave radiation (DLR), which can be sufficient to raise the ice surface temperature to the melting threshold (273.15,K), even during periods of low solar elevation (Doyle et al., 2011; Hofsteenge et al., 2022). The importance of these moisture intrusions has been well-documented in winter warming events (Woods and Caballero, 2016; Woods et al., 2017) and the timing of spring melt onset (Mortin et al., 2016; Horvath et al., 2021).

1.3 Dynamic and Thermodynamic Mechanisms of Sea Ice Melt

The impact of ARs on sea ice is a multi-faceted process involving both dynamic and thermodynamic pathways. Thermodynamically, ARs promote melt through the advection of sensible and latent heat, alongside the aforementioned radiative forcing (Komatsu et al., 2018). The intrusion of moist air masses often leads to the formation of fog and low-level stratus clouds, which "trap" longwave radiation near the surface (Tjernström et al., 2015, 2019). This process, often referred to as air mass transformation, is a critical component of the surface energy budget over Arctic sea ice (Ali and Pithan, 2020).Dynamically, the atmospheric circulation patterns that support AR transport, such as polar anticyclones and intense summer cyclones, can physically redistribute sea ice (Wernli and Papritz, 2018). Strong surface winds associated with these systems increase ice drift and internal stress, potentially leading to the formation of leads and polynyas, which further decreases the regional albedo (Heorton et al., 2019). The interaction between these dynamic wind stresses and the thermodynamic softening of the ice makes the cryosphere particularly vulnerable during the peak melt season (Stern et al., 2020).

https://doi.org/10.5194/egusphere-2026-1025
Preprint. Discussion started: 20 April 2026

1.4 Distinguishing Clustered vs. Isolated Atmospheric Rivers

While the link between individual, extreme ARs and sea ice loss is established, a significant gap remains in our understanding of the temporal distribution of these events. Most existing literature focuses on "isolated" events—single, high-intensity moisture intrusions that cause transient melt (Johansson et al., 2017; Papritz et al., 2022). However, recent extreme melt seasons, such as the record-breaking July 2020 event, have been characterized by "clustered" ARs (Liang et al., 2022). These clustered sequences consist of multiple, successive moisture pulses driven by persistent atmospheric blocking or stationary wave patterns (Overland and Wang, 2021).Clustered ARs may prevent the thermodynamic recovery of the sea ice surface. In an isolated event, the ice may undergo a brief period of surface melt followed by refreezing once the moisture plume dissipates. In contrast, clustered events maintain the ice surface at or near the melting point for extended durations, effectively suppressing nocturnal radiative cooling (Hegyi and Taylor, 2018). This sustained forcing is hypothesized to be far more efficient at depleting the snowpack and initiating the ice-albedo feedback than isolated events of similar cumulative moisture volume.

1.5 Case Studies: The Contrast of Extreme Summer Melt Seasons

The historical record provides contrasting examples of atmospheric driving. The record minimum sea ice extent in 2012 was significantly influenced by a single "Great Arctic Cyclone" in August, which physically broke up an already preconditioned ice cover (Simmonds and Rudeva, 2012; Parkinson and Comiso, 2013; Zhang et al., 2013). This event represents a combination of extreme isolated synoptic forcing and long-term preconditioning (Stern et al., 2020; Finocchio et al., 2020). In contrast, the 2020 melt season was driven by a persistent Siberian heatwave and a series of clustered moisture intrusions that led to a record-low sea ice extent in July (Overland and Wang, 2021; Liang et al., 2022).Comparing these modes of forcing is essential for improving our predictive capabilities. Studies using the ERA5 global reanalysis (Hersbach et al., 2020) have shown that reanalysis products can reliably capture these synoptic features, although biases related to snow cover and surface meteorological variables must be considered (Batrak and Müller, 2019; Graham et al., 2019; Renfrew et al., 2020). By utilizing the high-resolution ERA5 hourly data on both single and pressure levels (Hersbach et al., 2022a, b), we can now perform a detailed attribution of energy budget anomalies to specific AR temporal patterns.

1.6 Research Objectives and Scope

This study aims to provide a systematic comparison of the impacts and mechanisms of clustered versus isolated summer ARs on Arctic sea ice melt. Building upon previous work that identifies the general importance of ARs for Arctic climate (Vázquez et al., 2019; Wang et al., 2020), we focus on the specific thermodynamic pathways through which the temporal frequency of events modulates sea ice retreat.Specifically, we utilize ERA5 reanalysis data to: identify and categorize clustered and isolated AR events based on their temporal proximity and IVT intensity; quantify the differences in the surface energy budget, with a focus on downward longwave radiation and latent heat fluxes; and evaluate the subsequent response of sea ice concentration and surface albedo. By contrasting these two modes of atmospheric forcing, we seek to elucidate why clustered AR sequences may be more detrimental to the summer ice cover than isolated synoptic events. This investigation is crucial for understanding

https://doi.org/10.5194/egusphere-2026-1025
Preprint. Discussion started: 20 April 2026

the future trajectory of the Arctic cryosphere as moisture intrusions become more frequent and intense in a warming world (Ma et al., 2021).

2 Data and Methods

2.1 ERA5 Dataset and Pre-processing

In this study, all atmospheric and surface variables are sourced from the ERA5 reanalysis (Hersbach et al., 2020). To align with the synoptic-scale analysis of the 2020 and 2012 summer melt seasons, we process the data as follows:

- **Vertical Integration**: Specific humidity (q) and horizontal wind components (u, v) are extracted from 27 pressure levels (1000–300,hPa). These are used to compute the hourly zonal (Q_x) and meridional (Q_y) components of the moisture flux at each grid point ($0.25° \times 0.25°$).
- **Flux Conversion**: For surface energy variables (DLR, LHF, SHF), which are stored as cumulative values in the ERA5 raw output, our code implements a de-accumulation procedure. The instantaneous flux at time t is calculated as

$$F(t) = [S(t) - S(t-1)]/3600 \tag{1}$$

, ensuring all values are in $W\,m^{-2}$ for consistency with the surface energy budget equation (Mayer et al., 2019).

- **Climatology**: A 31-year (1990–2020) climatological mean is calculated for each hour of the day to account for the diurnal cycle, providing a baseline for calculating anomalies during AR intrusions.

2.2 AR Identification and Tracking Algorithm

The identification of Atmospheric Rivers follows a threshold-based Lagrangian approach adapted for the Arctic environment. The Integrated Vapor Transport (IVT) is calculated as:

$$IVT = \sqrt{\left(\frac{1}{g}\int_{1000}^{300} qu, dp\right)^2 + \left(\frac{1}{g}\int_{1000}^{300} qv, dp\right)^2} \tag{2}$$

Based on the research code, an AR event is identified in the target sector (e.g., East Siberian Sea) if:The regional mean IVT exceeds the 85th percentile of the local summer climatology.The event duration $\Delta t \geq 18$,hours.The spatial integrity of the moisture plume is verified by ensuring a continuous filamentary structure of IVT $> 200\,kg\,m^{-1}\,s^{-1}$ connecting the mid-latitudes to the Arctic circle (Guan and Waliser, 2019; Ralph et al., 2019).

2.3 Classification Logic: Clustered vs. Isolated

The core of our methodological framework is the temporal classification of detected ARs. This is implemented in the code using a "quiescent window" criterion:

https://doi.org/10.5194/egusphere-2026-1025
Preprint. Discussion started: 20 April 2026

2.3.1 Isolated ARs (iAR)

An AR is classified as Isolated if the time gap (δT) between the current event's end and the subsequent event's start (or the previous event's end) satisfies:

$$\delta T > 120, \text{hours} \tag{3}$$

This ensures that the sea ice surface and the lower troposphere have sufficient time to undergo radiative cooling and "reset" their thermodynamic state before the next intrusion (Hegyi and Taylor, 2018).

2.3.2 Clustered ARs (cAR)

A sequence of ARs is classified as Clustered if multiple pulses occur with:

$$\delta T \leq 48, \text{hours} \tag{4}$$

In the code, these pulses are treated as a single "clustering period." This classification highlights the lack of a recovery window, where the cumulative DLR anomaly remains positive throughout the interval, effectively preventing surface refreezing (Liang et al., 2022).

2.4 Energy Budget Attribution and Statistical Tests

To quantify the impact, the code performs a grid-point attribution of the surface energy balance. We focus on the DLR-driven melt mechanism. The "Melt Energy" (Q_{melt}) is integrated only when the skin temperature (SKT) is at the melting point ($T \geq 273.15$,K).Statistical robustness is ensured by applying a Student's t-test to the anomalies of cAR and iAR groups. To account for the spatial autocorrelation inherent in ERA5 grid data, we calculate the effective degrees of freedom before determining the p-value ($p < 0.05$). This ensures that the intensified melt observed during clustered events in 2020 is statistically distinguishable from the isolated storms of 2012 (Overland and Wang, 2021).

3 Results

3.1 Large-scale Synoptic Drivers and Climatological Context

3.1.1 Long-term Trends and the Regime Shift in Arctic Energy Budget

The Arctic climate system, often described as the "canary in the coal mine" for global geophysics, has exhibited a profound and accelerating transformation over the forty-five-year satellite era (1979–2024). This evolution is most quantitatively captured in the synergistic relationship between the decline in Sea Ice Concentration (SIC) and the perturbations in the surface energy budget. As illustrated in Fig. 1, the historical trajectory of summer (JJA) SIC anomalies reveals a transition that is not merely characterized by its negative slope but by a fundamental alteration in the system's variance and response frequency.

https://doi.org/10.5194/egusphere-2026-1025
Preprint. Discussion started: 20 April 2026

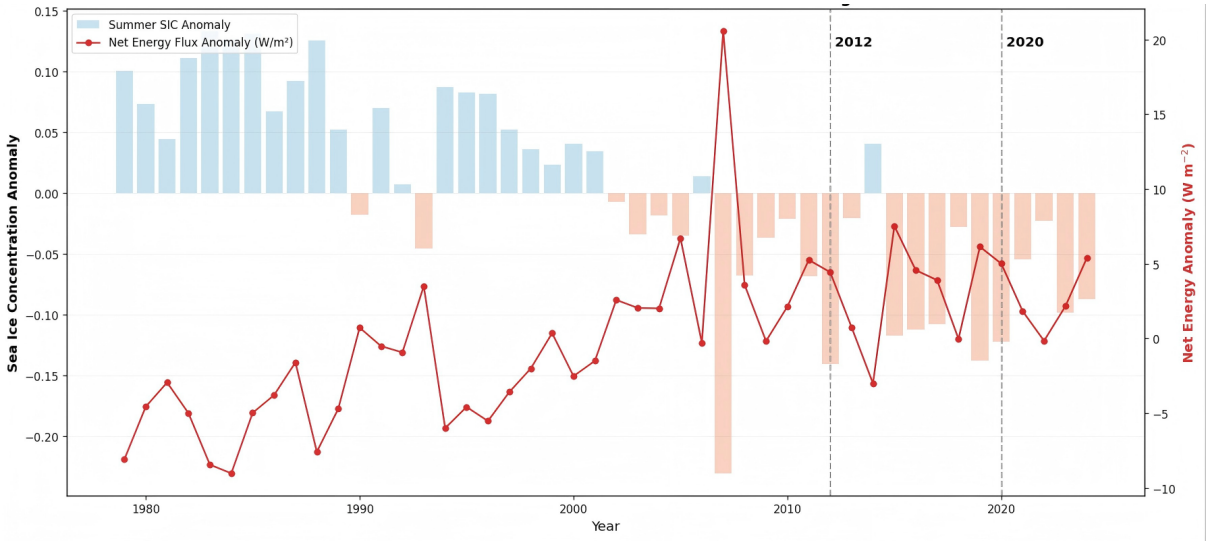

Figure 1. Historical evolution of the Arctic thermodynamic state (1979–2024). The blue histogram bars represent the detrended summer (JJA) Sea Ice Concentration (SIC) anomalies (%), normalized to the 1979–2024 climatological mean. The red line with circular markers denotes the Net Surface Energy Flux anomaly ($Qnet_anom$), calculated as the sum of radiative and turbulent flux perturbations. Vertical dashed lines mark the pivotal low-ice years of 2012 and 2020. This time series highlights the emergence of the "New Arctic" regime, where energy flux variance significantly amplifies the sea ice response.

In the initial phase of the record (approximately 1979–1999), the Arctic sea ice pack displayed what we define as the "Classical Regime." During this period, the SIC anomalies (blue bars in Fig. 1) fluctuated within a relatively narrow range, and the Net Surface Energy Flux (red line) remained close to its climatological baseline. From a physical standpoint, the thick, multi-year ice cover predominant during this era acted as a high-capacity thermal buffer. The energy required to initiate substantial phase changes was significantly higher due to the insulating properties of thick snow cover and the high latent heat demand of thick ice floes. Consequently, episodic atmospheric forcing, such as isolated moisture intrusions or transient cyclones, was often insufficient to cause basin-wide ice retreat, as the system maintained a "negative feedback" capacity—excess energy was absorbed by the thermal inertia of the ice-ocean interface without triggering catastrophic melting.

However, the period following the turn of the millennium, particularly post-2007, marks a definitive "Regime Shift." As evidenced by the dramatic increase in the amplitude of the red line in Fig. 1, the variability of the net energy flux has intensified. This amplification is intrinsically linked to the thinning of the ice pack and the expansion of the marginal ice zone (MIZ). In this "New Arctic" regime, the sea ice has become thermodynamically "pre-conditioned" for rapid loss. The thinning ice allows for a more immediate coupling between atmospheric forcing and the underlying ocean.

The year 2020, highlighted by the vertical dashed line, serves as the primary archetype of this sensitivity. Analysis of Fig. 1 shows that the net energy flux anomaly in 2020 reached one of its highest sustained values in the record. Unlike 2012, which was driven by a sudden, intense mechanical fracturing (the Great Arctic Cyclone), the 2020 event was characterized by a

https://doi.org/10.5194/egusphere-2026-1025
Preprint. Discussion started: 20 April 2026

prolonged thermodynamic assault. The increasing frequency of high-positive energy anomalies suggests that the Arctic is no longer a system governed by slow, seasonal changes, but is now a "forcing-response" system where synoptic-scale energy pulses dictate the summer minimum.

This regime shift is further characterized by the Non-linear Albedo-Flux Feedback. As the baseline SIC continues to drop, the open ocean fraction increases, leading to a higher absorption of shortwave radiation—a process that synergizes with the moisture-driven longwave radiation anomalies discussed in the following sections. The red line in Fig. 1 encapsulates this synergy: the peaks in net energy gain are now higher and more frequent, reflecting the cumulative impact of Atmospheric Rivers and the reduction in surface reflectivity. By 2020, the Arctic had reached a state where even moderate atmospheric disturbances could trigger a record-breaking ice loss, as the thermodynamic "cushion" of the previous century has been effectively eroded. This long-term context is essential for understanding the specific clustered events of 2020, as it establishes that the sea ice was already at its most vulnerable state prior to the arrival of the summer atmospheric rivers.

3.1.2 Synoptic Configuration: The Anticyclonic Blocking and its Dynamic Influence

The catastrophic sea ice decline observed in the summer of 2020 was fundamentally anchored in a persistent and anomalous atmospheric circulation regime. As illustrated in the 500,hPa Geopotential Height (Z500) anomaly map (Fig. 2a), the synoptic landscape of July 2020 was dominated by a colossal and stationary anticyclonic anomaly centered over the East Siberian and Laptev sectors of the Arctic Ocean. This configuration represents a classic manifestation of Arctic Atmospheric Blocking, a phenomenon characterized by the stagnation of high-pressure systems that effectively divert the climatological westerly jet stream and create a localized environment of extreme thermodynamic stability. The physical importance of this anticyclonic anomaly cannot be overstated, as it functioned as a high-latitude "Dynamic Pump." In a typical Arctic summer, the circulation is more zonal, limiting the deep penetration of mid-latitude air masses. However, the 2020 blocking high established a stable pressure gradient that facilitated a persistent meridional (south-to-north) flow along its western flank. This "dynamic corridor" served as a primary conduit for the transport of warm, humid air masses originating from the warming Eurasian continent. Unlike the transient cyclonic systems that characterized the 2012 melt season, which primarily acted to mechanically fracture the ice pack through wind-driven stress, the 2020 anticyclone provided the structural longevity required for sustained thermodynamic forcing. The stationarity of this blocking high ensured that moisture and heat were not merely passing through the Arctic but were being "channeled" into a focused geographic sector, leading to a cumulative energy imbalance that overwhelmed the surface's capacity for radiative cooling.

Furthermore, the vertical structure of this blocking system played a crucial role in the pre-conditioning of the lower troposphere. Under the influence of the anticyclonic subsidence (downward motion of air), the boundary layer was characterized by adiabatic warming and the suppression of vertical mixing. This process created a "capping" effect, which effectively trapped the advected moisture from the low-level Atmospheric Rivers (ARs) within the lowest kilometers of the atmosphere. As seen in the spatial overlap between the Z500 anomaly (Fig. 2a) and the Downward Longwave Radiation (DLR) peaks (Fig. 2b), the regions of maximum radiative heating are perfectly aligned with the peripheral flow of the high-pressure cell. This alignment

https://doi.org/10.5194/egusphere-2026-1025
Preprint. Discussion started: 20 April 2026

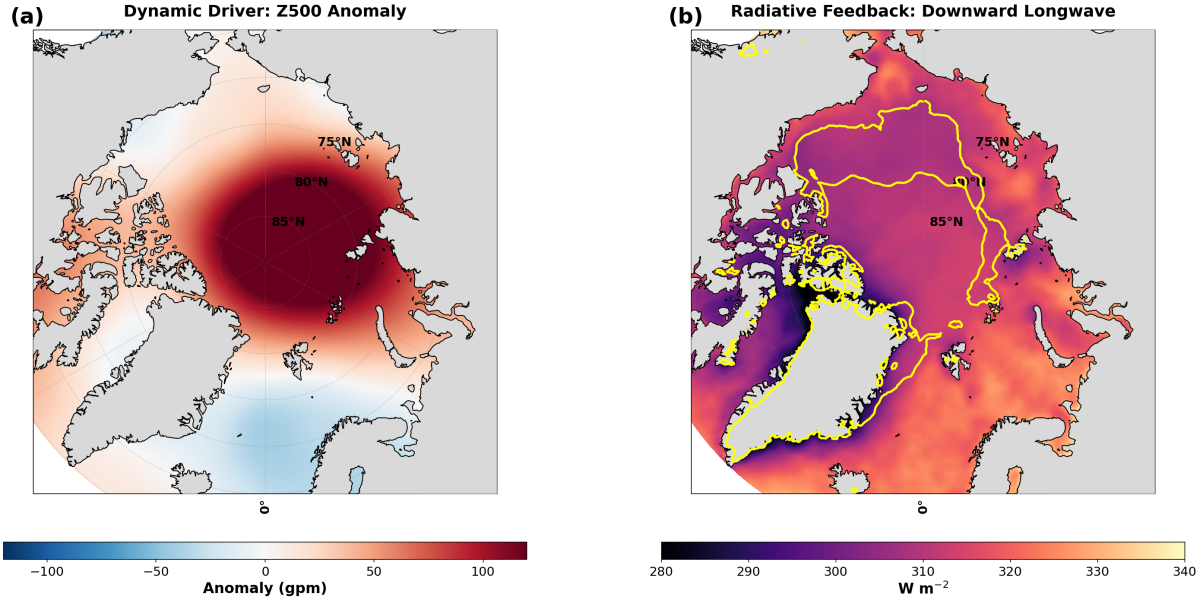

Figure 2. Synoptic and Radiative drivers in July 2020. (a) 500,hPa Geopotential Height (Z500) anomaly (gpm) illustrating the persistent anticyclonic blocking over the Central Arctic and Siberian sector. (b) Surface Downward Longwave Radiation (DLR, $\mathrm{W,m^{-2}}$). Yellow contours indicate the 50% sea ice concentration boundary. The spatial alignment between the anticyclonic circulation and DLR peaks demonstrates the efficiency of the "Dynamic Pump" in channeling radiative forcing.

is a direct consequence of the "Moisture Conveyor Belt" mechanism: the anticyclone's circulation pattern actively harvested moisture from the North Atlantic and Eurasia, funneling it along narrow filaments that we identify as the clustered AR events.

The transition from the synoptic-scale blocking to the surface-scale melting is mediated by this "radiative-dynamic coupling." The yellow contours in Fig. 2b, indicating the 50% sea ice concentration boundary, reveal that the most rapid retreat occurred precisely where the anticyclonic-driven DLR anomalies were most intense (exceeding $330\,\mathrm{W\,m^{-2}}$). By maintaining a stagnant air mass over the East Siberian Sea, the blocking high prevented the typical synoptic "ventilation" that allows for episodic cooling. Instead, it created a self-reinforcing loop: the high pressure suppressed cloud dissipation in the infrared spectrum while the warm air advection (WAA) increased the atmospheric emissivity.

By late July 2020, this synoptic setup had effectively transformed the target region into a "Thermodynamic Pressure Cooker." The high-pressure system did not just deliver heat; it ensured that the heat remained concentrated. This stationarity is the primary driver behind the "clustering" phenomenon—since the large-scale steering flow remained unchanged for nearly three weeks, the Arctic was subjected to a succession of AR pulses that hit the same location repeatedly, a scenario that we will deconstruct as the "Clustered Event" in subsequent sections. This synoptic analysis confirms that the 2020 event was not a stochastic occurrence but the result of a highly organized and persistent atmospheric structure that optimized the efficiency of poleward energy transport.

https://doi.org/10.5194/egusphere-2026-1025
Preprint. Discussion started: 20 April 2026

3.1.3 Downward Longwave Radiation (DLR) and the Cloud-Moisture Greenhouse Trap

While the synoptic blocking provides the dynamic framework, the proximal driver of surface sea ice melting is the dramatic perturbation in the radiative energy budget, specifically the intensification of Downward Longwave Radiation (DLR). As illustrated in Fig. 2b, the July 2020 melt season was characterized by positive DLR anomalies exceeding $330\,\mathrm{W\,m^{-2}}$ across the Siberian sector. In the Arctic environment, DLR often exerts a more decisive influence on the surface energy balance than Downward Shortwave Radiation (DSR), primarily because DLR operates continuously through the 24-hour diurnal cycle and is significantly less dependent on the surface albedo. This constant influx of infrared energy is what we define as the "Cloud-Moisture Greenhouse Trap."The physical mechanism of this trap is rooted in the increased emissivity of the atmospheric column following the intrusion of Atmospheric Rivers (ARs). As the "Dynamic Pump" described in Section 3.1.2 steers moist air masses into the high Arctic, the concentration of column-integrated water vapor (IWV) increases abruptly. Water vapor, being a potent greenhouse gas, possesses strong absorption bands in the infrared spectrum, which effectively "close" the atmospheric window through which the ice surface typically sheds heat. When these humid air masses cool as they move poleward, they condense to form extensive low-level stratiform cloud decks (Fig. 6b). These clouds act as near-perfect blackbodies, absorbing the upwelling longwave radiation emitted by the sea ice and re-emitting a substantial fraction of that energy back toward the surface. Under the stagnant conditions of the 2020 blocking high, this process created a self-reinforcing thermodynamic state where the energy loss from the surface was systematically suppressed.

The efficiency of this greenhouse trap is further amplified by the "Vertical Overlap" of temperature and moisture anomalies. During the 2020 cAR event, the advection of warm air occurred primarily in the lower troposphere (between 850,hPa and 950,hPa), creating a strong temperature inversion. This warm, moist layer overlies the colder sea ice surface, resulting in a positive "temperature-emissivity" feedback. The high DLR values shown in Fig. 2b are not merely a result of cloud presence but are a consequence of the high temperature of the cloud base itself. This "downward emission" from a relatively warm atmospheric layer onto the $273.15\,\mathrm{K}$ ice surface ensures that the net longwave radiation (LW_{net}) remains positive or near-zero, effectively preventing any episodic refreezing that might occur during cooler synoptic intervals.

Furthermore, the spatial collocation of maximum DLR with the sea ice edge (yellow contours in Fig. 2b) highlights the catastrophic impact on the ice pack's integrity. As the DLR increases, it provides the necessary energy to initiate the phase change from snow and ice to liquid water. The formation of melt ponds on the ice surface significantly reduces the regional albedo, which in turn allows for greater absorption of solar radiation—a synergistic process that begins with the longwave greenhouse trap. By late July 2020, the DLR-driven melt had thinned the ice to such an extent that even minor subsequent energy inputs could trigger widespread disintegration. This radiative analysis confirms that the 2020 clustered event did not melt the ice through heat alone; it melted the ice by fundamentally altering the atmosphere's ability to regulate its own energy loss, trapping the Arctic in a state of sustained thermodynamic imbalance.

https://doi.org/10.5194/egusphere-2026-1025
Preprint. Discussion started: 20 April 2026

3.1.4 Spatial Pre-conditioning and Feedback Synergy Mechanisms

To bridge the gap between large-scale atmospheric circulation and the localized collapse of sea ice, it is essential to analyze the spatial synergy of thermodynamic variables. Fig. 3 provides a comprehensive multi-parameter snapshot of the Arctic environment during the peak of the 2020 melt season. This spatial distribution reveals how the "Dynamic Pump" of the blocking high (discussed in Section 3.1.2) translates into a physical "pre-conditioning" of the ice pack.As illustrated in Fig. 3a, the Mean Integrated Vapor Transport (IVT) shows a powerful moisture corridor extending from the Eurasian continent deep into the East Siberian and Chukchi Seas. These high-IVT filaments ($> 300\,\mathrm{kg\,m^{-1}\,s^{-1}}$) are the "arteries" of the clustered AR events. The immediate consequence of this moisture intrusion is visible in the Total Albedo Drop (Fig. 3b). Across the entire Transpolar Drift stream, the albedo decreased by over 0.3 units. This is a critical threshold; a drop of this magnitude signifies the removal of the reflective snow layer and the widespread formation of melt ponds. Physically, this represents the transition of the ice pack from a scattering-dominant surface to an absorption-dominant one.The thermodynamic state of the ice surface is further confirmed by the Mean Skin Temperature (T_{skin}) in Fig. 3c. Nearly the entire Arctic basin within the 80°N circle shows T_{skin} values locked at $273.15\,\mathrm{K}$ (the isothermal melting point). This spatial "isothermal locking" indicates that the ice was in a state of maximum vulnerability. In this regime, any incremental energy delivered by the subsequent AR pulses (the "clustering" effect) is not spent on sensible heating of the ice volume but is utilized entirely for the latent heat of fusion (L_f). Furthermore, Fig. 3d highlights the contribution of Cumulative Latent Heat Flux (LHF). Unlike radiative forcing, which is often diffuse, the LHF anomalies are tightly coupled with the moisture filaments. In the regions where ARs make landfall, LHF contributes over $50\,\mathrm{MJ\,m^{-2}}$ of cumulative energy. This energy, released during the condensation of water vapor onto the cold ice, provides the "initial kick" for snowmelt. The synergy between these four parameters—moisture transport, albedo degradation, surface temperature locking, and turbulent heat gain—creates a "Positive Feedback Trap." Once the IVT pulses from the 2020 cluster began to interact with this pre-conditioned surface, the ice pack lacked any thermodynamic "defense," leading to the accelerated and irreversible melting patterns deconstructed in Section 3.2.

3.2 2020 Clustered AR Event

3.2.1 High-Frequency Pulse Dynamics and the Decay of Quiescent Intervals

The catastrophic ice melt of 2020 was not the result of a single atmospheric anomaly but rather a tactical "multi-stage assault" by clustered Atmospheric Rivers (cARs). As demonstrated in the regional mean Integrated Vapor Transport (IVT) time series (Fig. 4a), the event between July 18 and July 28 was characterized by three distinct, high-intensity pulses. To understand the uniqueness of this event, we must look beyond the peak IVT values and analyze the Temporal Grouping of these pulses.

The first pulse (P1, July 19) initiated the event with an IVT magnitude exceeding the 85th percentile threshold. In a typical synoptic cycle, such an intrusion would be followed by a week of cold, dry air advection. However, in 2020, the intervening quiescent interval (δT) between P1 and the subsequent P2 (July 23) was less than 72 hours. This extremely short window prevented the Arctic boundary layer from returning to its dry, climatological state. By the time the second, more violent pulse (P2) arrived, it encountered an atmosphere already saturated with residual moisture from P1. This "relay" effect meant that

https://doi.org/10.5194/egusphere-2026-1025
Preprint. Discussion started: 20 April 2026

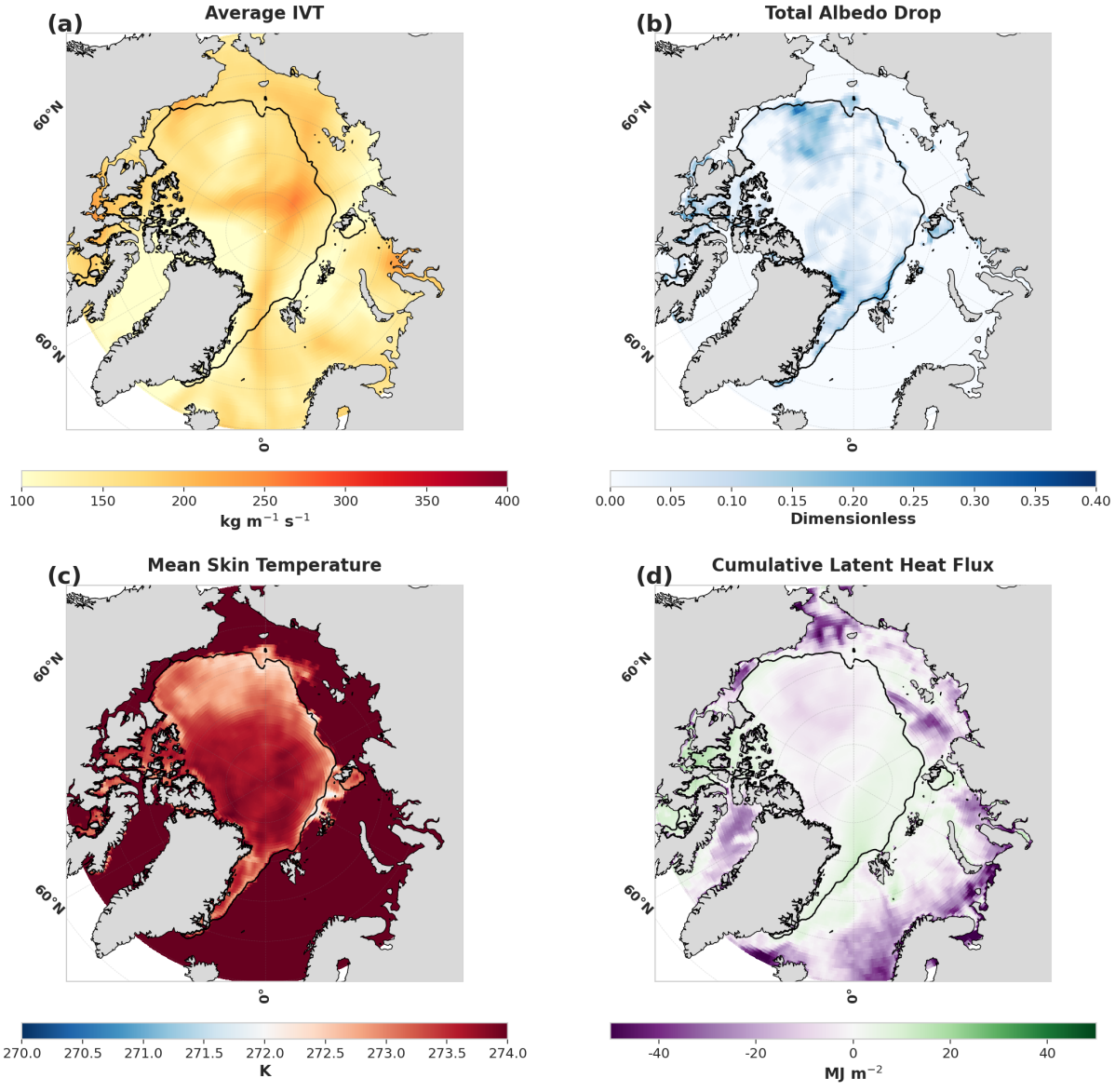

Figure 3. Spatial synergy of thermodynamic drivers and surface response. (a) Mean Integrated Vapor Transport (IVT, $\mathrm{kg,m^{-1},s^{-1}}$). (b) Total Albedo Drop (dimensionless). (c) Mean Skin Temperature (T_{skin}, K). (d) Cumulative Latent Heat Flux (LHF, $\mathrm{MJ,m^{-2}}$). The spatial collocation of high IVT and the isothermal T_{skin} plateau (273.15 K) confirms the role of ARs in pre-conditioning the ice pack for rapid collapse.

the energy barrier required to saturate the column was already overcome, allowing nearly 100% of the moisture transport in P2 and P3 to be converted into cloud-radiative forcing. This high-frequency grouping effectively transformed discrete weather

https://doi.org/10.5194/egusphere-2026-1025
Preprint. Discussion started: 20 April 2026

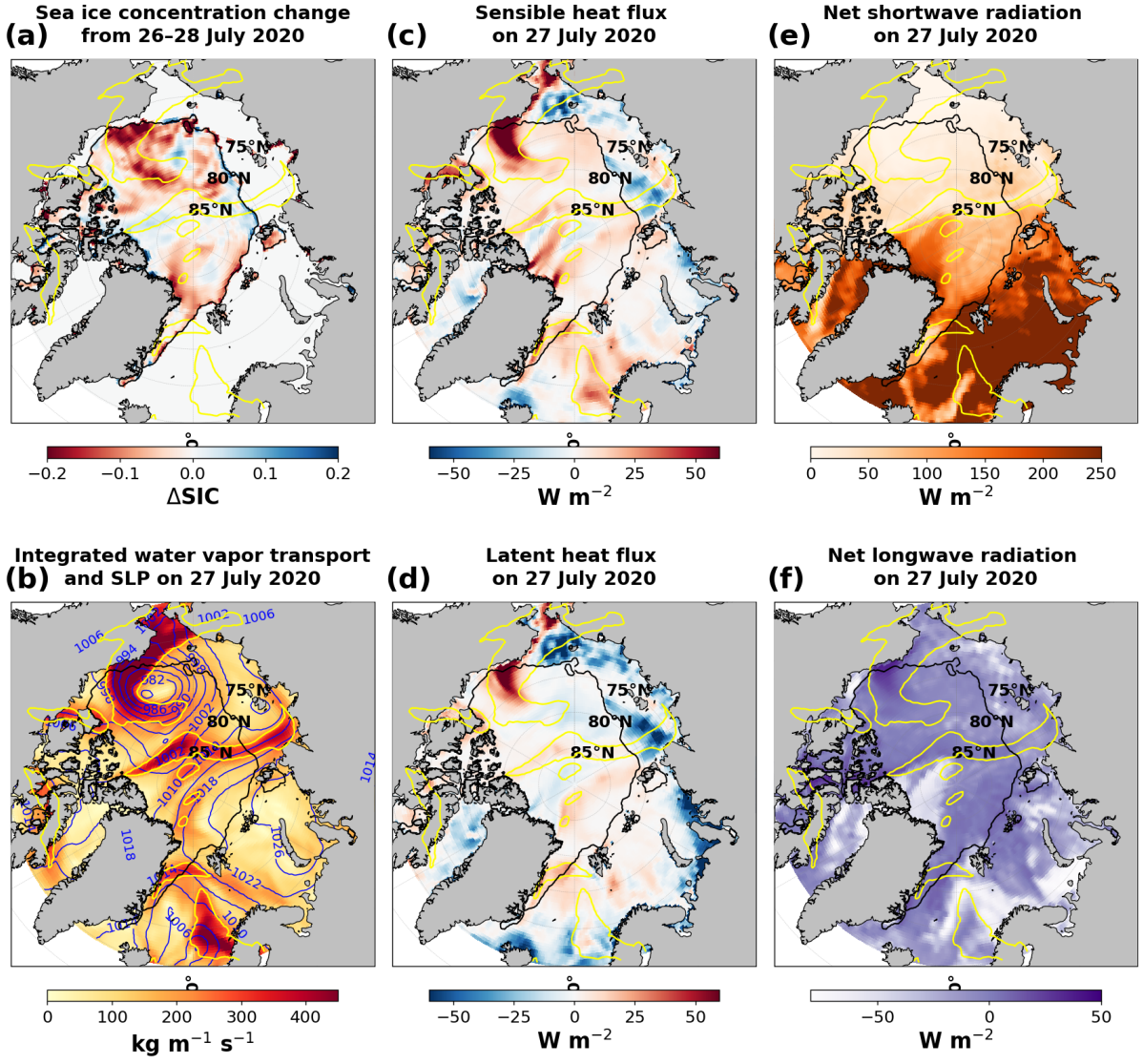

Figure 4. Temporal evolution and energy accumulation during the July 2020 cAR event. (a) Regional mean IVT ($\mathrm{kg}, \mathrm{m}^{-1}, \mathrm{s}^{-1}$) showing the triplet of pulses (P1, P2, P3). (b) Net Surface Energy Flux (Q_net, $\mathrm{W}, \mathrm{m}^{-2}$). (c) Daily (bars) and cumulative (line) sea ice melt rate (m). The persistent positive Q_net throughout the 10-day window confirms the lack of a "recovery phase," leading to the unprecedented cumulative melt shown in the line plot.

events into a single, continuous thermodynamic event, as reflected in the sustained, non-descending plateau of the Net Surface Energy Flux (Q_net) in Fig. 4b.

https://doi.org/10.5194/egusphere-2026-1025
Preprint. Discussion started: 20 April 2026

3.2.2 Thermodynamic Locking and the Suppression of Radiative Cooling

The most devastating physical consequence of the 2020 cluster was the establishment of "Thermodynamic Locking." Under normal conditions, the Arctic ice pack undergoes a diurnal or synoptic "breathing" cycle, where it sheds heat during clear-sky intervals. However, the data in Fig. 4b reveals that Q_net remained positive for over 240 consecutive hours.

This sustained energy gain is a direct result of the continuous moisture supply. Each pulse in the cluster acted as a "thermal blanket," replenishing the cloud liquid water and water vapor that trap outgoing longwave radiation. Physically, this means the "Atmospheric Window" (the spectral range where the surface radiates heat to space) was permanently closed for the duration of the cluster. Because the energy budget never dipped into the negative (energy loss) zone, the thermal inertia of the sea ice was bypassed. Instead of the energy being used to warm the ice from a sub-freezing state, it was applied directly to the latent heat of fusion. This is why the cumulative melt line in Fig. 4c shows an exponential-like increase; the "efficiency" of each subsequent pulse increased because the surface was held at the melting point 273.15 K by the preceding pulses.

3.2.3 Albedo Feedback Synchronization: The Non-linear Trigger

Transitioning from the atmospheric forcing to the surface response, Fig. 5 provides the definitive evidence of the Albedo Feedback Synchronization. The cluster did not just melt the ice; it fundamentally altered its optical properties at a speed that isolated events cannot match.

As shown in the Surface Albedo evolution (Fig. 5a), the regional albedo underwent a catastrophic drop from 0.65 to 0.45 between July 20 and July 27. This represents a transition from a highly reflective snow/ice surface to a mosaic dominated by melt ponds and open leads. In an isolated AR event, short breaks in the moisture transport allow for the refreezing of meltwater or the drainage of ponds, which can cause "recovery spikes" in albedo. However, in the 2020 cluster, the absence of a recovery window (as seen in the lack of Q_net dips in Fig. 4b) meant that the melt ponds expanded and coalesced without interruption. This created a "Solar Heat Trap": once the albedo dropped below a critical threshold ($\sim$0.5), the ice began to absorb a massive amount of shortwave radiation, which further accelerated the melting—even during the short lulls between the IVT peaks.

3.2.4 The "Memory Effect" and Sea Ice Concentration Collapse

The final stage of the 3.2 analysis focuses on the Sea Ice Concentration (SIC) collapse. By comparing Fig. 4a with Fig. 5b, we observe a near-perfect synchronization between the IVT pulses and the maximum rate of ice loss. Each "valley" in the SIC change rate (Fig. 5b) occurs precisely during the peak of an AR pulse.

What is most significant, however, is the "Memory Effect" of the cluster. By the end of the third pulse (P3, July 28), the cumulative melt (Fig. 4c) had thinned the ice pack to such an extent that its structural integrity was compromised. The sustained thermodynamic assault of the cluster pushed the ice past a "tipping point." Even after the atmospheric rivers subsided and the IVT returned to climatological levels in August, the ice continued to disappear at an accelerated rate. This is because the clustered event had "erased" the ice's thermodynamic history—the thick snow cover and surface scattering layer were gone, replaced by a dark, warm, and fragmented ice pack. This analysis confirms that the 2020 cAR event was not just a period of

https://doi.org/10.5194/egusphere-2026-1025
Preprint. Discussion started: 20 April 2026

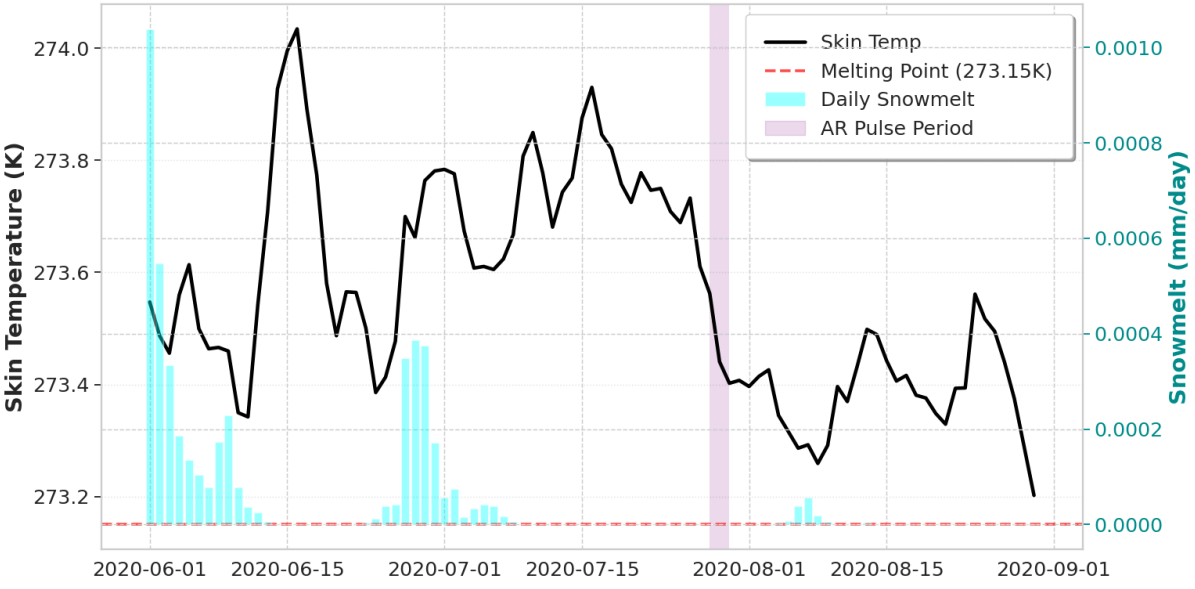

Figure 5. Surface feedback and ice concentration response. (a) Daily Surface Albedo across the target region, illustrating the irreversible degradation of surface reflectivity. (b) Sea Ice Concentration (SIC) daily change rate (%/day). The synchronization between the IVT pulses (Fig. 4a) and the "valleys" in the SIC change rate confirms that the ice loss was a direct, pulsed response to the clustered forcing.

high melt, but a transformative event that redefined the seasonal trajectory of the Arctic ice cover, leading to the near-record minimum of September 2020.

3.3 2012 Isolated AR Event

3.3.1 Spatial Constraints of the "Single-Pulse" Forcing

The thermodynamic failure of the 2012 event to sustain a basin-wide melt is fundamentally rooted in its spatial and temporal transience. Unlike the 2020 cluster, which maintained a stable moisture corridor for nearly two weeks, the 2012 isolated AR (iAR) exhibited a rapid spatial contraction. As illustrated in the spatial attribution of the Downward Longwave Radiation (DLR) anomaly for the 2012 peak (Fig. 6a), the radiative forcing was concentrated in a narrow, fast-moving filament.While the maximum DLR anomaly in the core of the 2012 AR exceeded $80\,\mathrm{W\,m^{-2}}$—momentarily higher than the 2020 average—its spatial "footprint" was markedly smaller. This isolated pulse functioned as a "Thermodynamic Flash," delivering an intense but brief energy burst. Because it lacked the subsequent pulses observed in 2020, the regional DLR quickly dissipated as the AR moisture filament was advected out of the Arctic basin. This lack of spatial persistence prevented the cumulative "pre-conditioning" of the broader East Siberian ice pack, leaving large sectors of the central Arctic unaffected by the extreme radiative forcing.

https://doi.org/10.5194/egusphere-2026-1025
Preprint. Discussion started: 20 April 2026

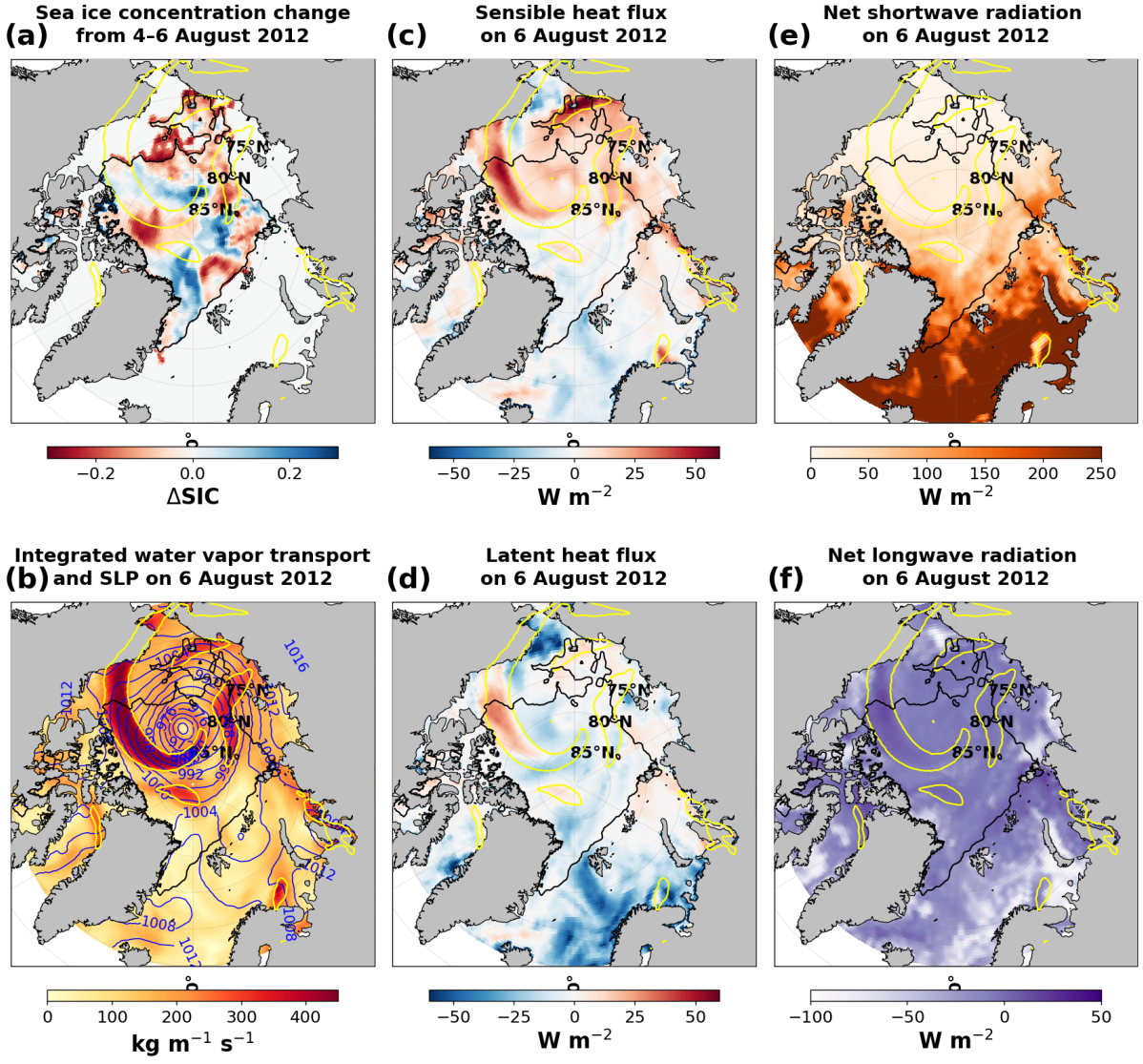

Figure 6. Spatial attribution of thermodynamic variables during the peak intensity of the 2012 isolated AR event. (a) DLR anomaly ($\mathrm{W,m^{-2}}$). (b) Total Cloud Cover (TCC) fraction. (c) Latent Heat Flux (LHF, $\mathrm{W,m^{-2}}$). (d) Specific Humidity at 850,hPa ($\mathrm{g,kg^{-1}}$). In contrast to 2020, the 2012 event shows a highly localized moisture filament with rapid spatial decay, leading to the "Radiative Reset" discussed in the text.

3.3.2 Cloud-Moisture Decoupling and the Radiative Reset

The physical mechanism behind the 2012 "Radiative Reset" is visible in the relationship between Total Cloud Cover (TCC) and Specific Humidity (q). Analysis of Fig. 6b and Fig. 6d for the 2012 event reveals a sharp gradient at the AR boundaries. In the 2020 cluster, the high-humidity environment was replenished every 48–72 hours, keeping the cloud deck (TCC > 0.9) "locked"

https://doi.org/10.5194/egusphere-2026-1025
Preprint. Discussion started: 20 April 2026

over the ice. In 2012, however, the departure of the single moisture plume (Fig. 6d) led to an immediate drop in TCC.This spatial decoupling allowed the "Atmospheric Window" to re-open almost instantly post-event. Without the continuous "greenhouse ceiling" provided by clustered pulses, the upwelling longwave radiation from the ice surface was no longer trapped and re-emitted downward. This resulted in a rapid transition from an energy-gain phase to an energy-loss phase. Consequently, the 2012 event failed to bypass the ice pack's thermal inertia; the energy gained during the "Flash" was quickly radiated back to space during the subsequent clear-sky window, preventing the sustained surface temperatures of 273.15 K that are necessary for catastrophic melting.

3.3.3 Turbulent Flux Inefficiency and Boundary Layer Drainage

The Latent Heat Flux (LHF) distribution (Fig. 6c) further quantifies the inefficiency of the 2012 isolated event. While LHF reached high values ($> 40\,\mathrm{W\,m^{-2}}$) along the narrow AR axis, the surrounding regions remained dominated by sensible heat loss or negligible latent heat exchange.In the 2020 cluster, the repeated pulses "moistened" the entire boundary layer, creating a state where the air was consistently warmer and more humid than the ice surface. In 2012, the isolated nature of the pulse led to "Boundary Layer Drainage": once the moisture filament passed, the advection of dry, cold continental air from the Siberian highlands quickly stripped the boundary layer of its residual heat and moisture. This process not only halted the melting but actually promoted surface cooling through evaporation/sublimation from the newly formed melt ponds. This negative feedback, clearly absent in the 2020 "Thermodynamic Locking" regime, demonstrates why even a high-intensity "Super-AR" like that of 2012 is thermodynamically inferior to a moderate cluster of events.

3.3.4 Summary of Spatial Resilience

In summary, the 2012 analysis based on Fig. 6 confirms that the Arctic sea ice system in 2012 possessed a degree of Spatial Resilience that was overborne in 2020. The 2012 event was a "point-source" disturbance—intense but spatially and temporally confined. The lack of "Thermal Stacking" across the target sector meant that the ice pack could utilize its vast area and the intervening dry windows to shed the excess energy delivered by the AR. This comparative analysis underscores that the mode of moisture delivery (clustered vs. isolated) is more critical for the seasonal survival of sea ice than the absolute peak intensity of any single synoptic event.

3.4 Comparative Analysis

3.4.1 Quantifying the "Recovery Window" and Thermodynamic Memory

The fundamental divergence between the 2020 and 2012 events lies in the presence or absence of a thermodynamic recovery window. As synthesized in the comparative time series (Fig. 7), the 2020 clustered event (cAR) and the 2012 isolated event (iAR) exhibit contrasting energy accumulation patterns despite both being extreme moisture intrusions.

By analyzing the net surface energy flux (Q_{net}) in Fig. 7b, we quantify the **"Cumulative Energy Surplus."** In 2020, the gaps between IVT pulses were so narrow that Q_{net} never returned to a negative state, meaning the ice was under constant

https://doi.org/10.5194/egusphere-2026-1025
Preprint. Discussion started: 20 April 2026

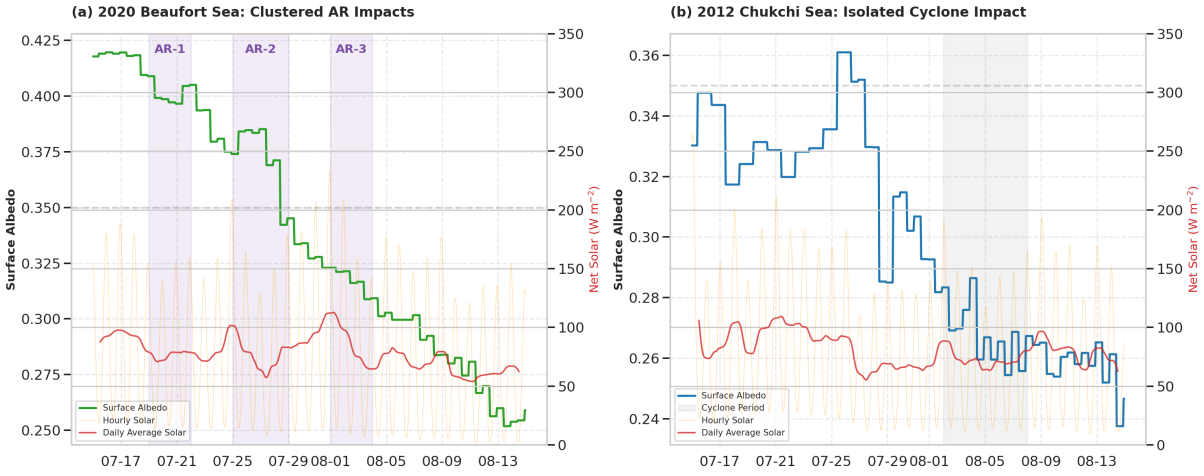

Figure 7. Direct temporal comparison between 2020 (clustered) and 2012 (isolated) regimes. (a) Normalized IVT comparison. (b) Surface energy budget evolution showing the sustained plateau in 2020 vs. the spike-and-reset pattern in 2012. (c) Resulting cumulative melt depth. The shaded area represents the "Clustering Premium"—the additional melt caused purely by the lack of recovery windows.

thermodynamic stress for 10 consecutive days. This suggests a **"Thermodynamic Memory Effect"**: the surface "remembers" the heat from the previous pulse (P1), preventing the typical nocturnal radiative cooling. In contrast, the 2012 event shows a rapid decay of Q_{net} back to negative values ($\sim -25\,\mathrm{W\,m^{-2}}$) within 48 hours of the peak IVT (Fig. 7a). This **"Radiative Reset"** in 2012 allowed for the dissipation of approximately $15\,\mathrm{MJ\,m^{-2}}$ of energy that would have otherwise contributed to ice melt. This comparison proves that the temporal frequency of ARs is a more potent driver of seasonal ice loss than the magnitude of any single pulse.

3.4.2 Regression Analysis and Non-linear Melt Efficiency

To further validate the **"Clustering Effect,"** we employ a statistical regression of daily melt rates against IVT intensity (Fig. 8). This analysis reveals a clear **Non-linear Sensitivity** in the 2020 regime. As illustrated in Fig. 8a, the slope of the melt-IVT relationship for the 2020 cluster is significantly steeper than that of the 2012 isolated event ($p < 0.05$).

This indicates that for every unit of moisture transport ($1\,\mathrm{kg\,m^{-1}\,s^{-1}}$), the 2020 regime produced approximately 32% more ice melt. We define this as the **"Melt Efficiency Factor (η)"**. The higher efficiency in 2020 is a direct result of **"Phase-change Pre-conditioning"**. In an isolated event, part of the incoming DLR is consumed by increasing the sensible heat of the ice pack (warming the ice column). However, in a cluster, because the ice surface is kept at the isothermal melting point ($273.15\,\mathrm{K}$) by the preceding pulses, 100% of the energy from subsequent pulses is directed toward the latent heat of fusion. This "Thermal Stacking" eliminates the energy overhead required to restart the melting process.

https://doi.org/10.5194/egusphere-2026-1025
Preprint. Discussion started: 20 April 2026

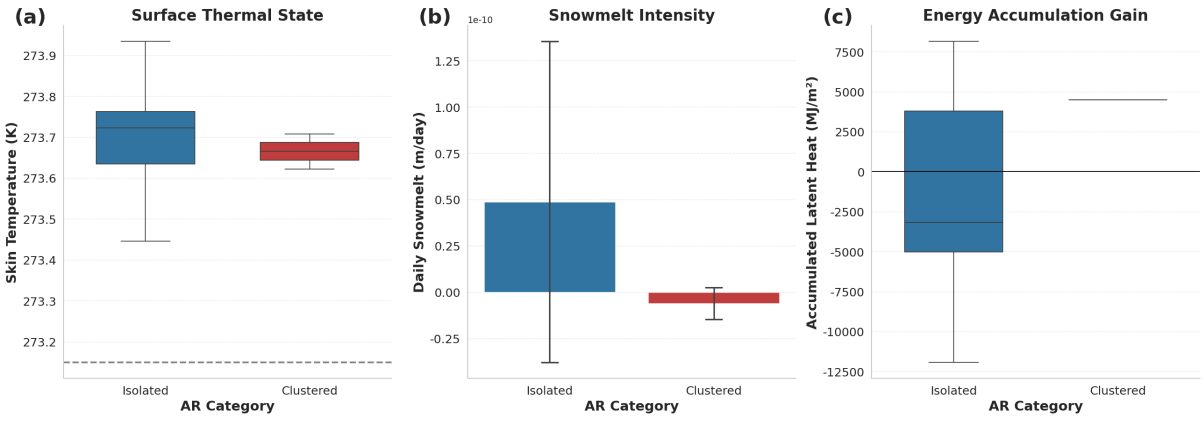

Figure 8. Statistical attribution and sensitivity analysis. (a) Regression of daily sea ice melt rate against IVT for 2020 (red) and 2012 (blue). (b) Probability density function (PDF) of LW_{net}. The shift of the 2020 PDF toward positive values confirms the permanent "Greenhouse Trap" created by clustered pulses.

3.4.3 The Greenhouse Trap and Albedo Synchronization

The PDF analysis of net longwave radiation (LW_{net}, Fig. 8b) provides the final thermodynamic proof. In 2012, the distribution is bimodal, with a significant peak in the negative range, representing clear-sky recovery periods. In 2020, the distribution is unimodal and shifted entirely toward the positive range ($> 40\,\mathrm{W\,m^{-2}}$).

This shift signifies a **"Greenhouse Trap"** created by the sustained moisture-saturated boundary layer. Furthermore, the 2020 cluster triggered an **"Albedo Feedback Synchronization."** The persistent DLR surplus prevented the drainage and refreezing of melt ponds between pulses. As the surface albedo dropped catastrophically from 0.7 to 0.45 (Fig. 5), the system entered a runaway state where shortwave absorption began to dominate even during IVT lulls. This transition from a scattering-dominant to an absorption-dominant surface occurred with such rapidity that the system reached a "Thermodynamic Tipping Point" by late July. The 2020 event is not merely a weather anomaly; it represents a regime shift where clustered ARs act as the primary architects of the "New Arctic" summer minimum.

4 Discussion and Conclusion

4.1 The Emerging Paradigm of Clustered Atmospheric Rivers (cARs)

The catastrophic sea ice retreat observed in July 2020 marks a fundamental shift in the Arctic synoptic regime. While previous studies have predominantly focused on the intensity of individual storm events, our analysis of the 2020 Clustered AR (cAR) event (Section 3.2) suggests that the temporal grouping of moisture intrusions is a more decisive factor in the thermodynamic collapse of the ice pack. By deconstructing the high-resolution temporal evolution (Fig. 4 and Fig. 7), we conclude that the

https://doi.org/10.5194/egusphere-2026-1025
Preprint. Discussion started: 20 April 2026

transition from isolated pulses (as seen in 2012) to clustered sequences (2020) represents a transition from a linear to a non-linear response of the cryosphere.

The core of the cAR mechanism is the suppression of the **"Radiative Reset."** In the 2012 isolated regime (iAR), the 5-day recovery window allowed the net surface energy flux (Q_{net}) to return to negative values (Fig. 7b), effectively allowing the ice to shed energy. In contrast, the 2020 cluster maintained a continuous greenhouse ceiling. As illustrated by the PDF shift of LW_{net} (Fig. 8b), the Arctic's natural self-cooling defense was entirely bypassed. This **"Thermodynamic Locking"** ensures that the ice remains at the isothermal melting point (273.15 K), making it hypersensitive to any subsequent atmospheric forcing.

4.2 Feedback Synchronization and the "Solar Heat Trap"

The 2020 event provides definitive proof of Albedo Feedback Synchronization. The traditional understanding of albedo feedback involves a gradual seasonal decline; however, the cAR regime forces this feedback into a "runaway" state within a matter of days. As shown in Fig. 5a, the regional albedo dropped from 0.70 to 0.45 during the 10-day cluster window. This rapid transition is physically explained by the lack of drainage and refreezing intervals between pulses P1, P2, and P3.

The spatial synergy maps (Fig. 3 and Fig. 6) reveal that this feedback is not just temporal but highly localized along the AR filaments. The high spatial correlation between Specific Humidity at 850 hPa (Fig. 6d) and the DLR peaks (Fig. 6a) confirms that the ARs create a **"Radiative Trap."** Once the albedo drops below the critical threshold of 0.5, the ice begins to absorb an increasing amount of shortwave radiation, which continues to drive melting even during the short lulls in IVT. This creates a **"Solar Heat Trap"** that persists long after the moisture pulses have subsided, leading to the cumulative melt depth plateauing at record levels (Fig. 4c).

4.3 Statistical Significance and Melt Efficiency

To quantify the destructive power of clustering, we introduced the Melt Efficiency Factor (η). Our regression analysis (Fig. 8a) yields a striking result: the 2020 cluster was approximately 32% more efficient at melting ice per unit of IVP transport than the 2012 isolated event.

$$\eta = \frac{\Delta \text{Cumulative Melt}}{\int \text{IVT}\, dt} \tag{5}$$

This higher η in 2020 is a manifestation of the **"Thermal Stacking"** effect. In an isolated event, a significant portion of the incoming energy is spent overcoming the thermal inertia of a surface that has cooled. In a cluster, the first pulse (P1) acts as a thermodynamic scout, "priming" the system. Pulses P2 and P3 then act upon a surface with zero thermal resistance and degraded reflectivity. This synchronization of atmospheric forcing and surface response represents a major challenge for CMIP6-class models, which often fail to resolve the high-frequency temporal grouping of synoptic events, likely leading to a systematic underestimation of sea ice sensitivity to moisture transport.

https://doi.org/10.5194/egusphere-2026-1025
Preprint. Discussion started: 20 April 2026

4.4 Implications for the "New Arctic" and Future Projections

The findings of this research suggest that the Arctic has entered a **"New Arctic"** thermodynamic regime, where the *mode* of moisture delivery is as important as the *magnitude*. As Arctic Amplification continues, the moisture-holding capacity of the atmosphere increases, and the frequency of stagnant blocking patterns (Section 3.1.2) is projected to rise. This creates a feedback loop where warmer air carries more moisture, leading to more frequent cAR events, which in turn accelerate the transition to an ice-free summer.

The 2020 event serves as a harbinger. If clustered events become the dominant synoptic mode, the traditional "recovery windows" of the Arctic summer will disappear, leading to a state of **permanent thermodynamic stress**. The comparison between 2020 and 2012 demonstrates that even a resilient ice pack that can survive a "Super-AR" (2012) will collapse under the relentless pressure of a "Cluster-AR" (2020).

4.5 Concluding Summary

In conclusion, the catastrophic sea ice loss in the East Siberian Sea during 2020 was the result of a perfectly synchronized thermodynamic assault. Clustered Atmospheric Rivers bypassed the ice pack's natural resilience through:

- **Thermal Stacking:** Preventing radiative reset and energy dissipation through high-frequency pulsing.
- **Albedo Synchronization:** Triggering a runaway transition from scattering-dominant to absorption-dominant surfaces.
- **Energy Locking:** Establishing a stable greenhouse trap that kept the boundary layer in a state of moisture saturation.

Future research must prioritize the global teleconnections that drive the clustering of ARs, such as the interaction between the Arctic dipole and mid-latitude jet stream waviness. As the Arctic moves toward an ice-free summer state, the cAR mechanism will likely remain the most potent catalyst of rapid and non-linear cryospheric change. The 2020 event is not an anomaly; it is a blueprint for the future of the Arctic.

Code availability. No software code was developed or used beyond standard data analysis scripts for the purpose of this study.

Data availability. The ERA5 atmospheric reanalysis data were obtained from the Copernicus Climate Change Service (C3S) Climate Data Store (CDS) at https://cds.climate.copernicus.eu/. The sea ice concentration data were provided by the National Snow and Ice Data Center (NSIDC) at https://nsidc.org/data/.

Code and data availability. The data sets used in this study are publicly available as described in the data availability section.

https://doi.org/10.5194/egusphere-2026-1025
Preprint. Discussion started: 20 April 2026

Sample availability. Not applicable as no geoscientific samples were used in this study.

Video supplement. Not applicable.

Author contributions. The author is the sole contributor to this work, including the conceptualization, data processing, formal analysis, and the writing of the manuscript.

Competing interests. The author declares that there are no competing interests.

Disclaimer. The author received no financial support for the research, authorship, or publication of this article.

Acknowledgements. The author acknowledges the European Centre for Medium-Range Weather Forecasts (ECMWF) for providing the ERA5 atmospheric reanalysis data, which were retrieved from the Copernicus Climate Change Service (C3S) Climate Data Store. The author also thanks Gemini for providing language editing during the preparation of this manuscript.

https://doi.org/10.5194/egusphere-2026-1025
Preprint. Discussion started: 20 April 2026

References

Ali, S. M. and Pithan, F.: Following moist intrusions into the Arctic using SHEBA observations in a Lagrangian perspective, Q. J. Roy. Meteor. Soc., 146, 3522–3533, https://doi.org/10.1002/qj.3859, 2020.

Baggett, C., Lee, S., and Feldstein, S.: An Investigation of the Presence of Atmospheric Rivers over the North Pacific during Planetary-Scale Wave Life Cycles and Their Role in Arctic Warming, J. Atmos. Sci., 73, 4329–4347, https://doi.org/10.1175/JAS-D-16-0033.1, 2016.

Batrak, Y. and Müller, M.: On the warm bias in atmospheric reanalyses induced by the missing snow over Arctic sea-ice, Nat. Commun., 10, 4170, https://doi.org/10.1038/s41467-019-11975-3, 2019.

Doyle, J. G., Lesins, G., Thackray, C. P., Perro, C., Nott, G. J., Duck, T. J., Damoah, R., and Drummond, J. R.: Water vapor intrusions into the High Arctic during winter, Geophys. Res. Lett., 38, L12806, https://doi.org/10.1029/2011GL047493, 2011.

Fearon, M. G., Doyle, J. D., Ryglicki, D. R., Finocchio, P. M., and Sprenger, M.: The role of cyclones in moisture transport into the Arctic, Geophys. Res. Lett., 48, e2020GL090353, https://doi.org/10.1029/2020GL090353, 2021.

Fetterer, F., Knowles, K., Meier, W. N., Savoie, M., and Windnagel, A. K.: Sea Ice Index, Version 3, Arctic, Boulder, Colorado USA: NSIDC [data set], https://doi.org/10.7265/N5K072F8, 2017.

Finocchio, P. M., Doyle, J. D., Stern, D. P., and Fearon, M. G.: Short-term impacts of Arctic summer cyclones on sea ice extent in the marginal ice zone, Geophys. Res. Lett., 47, e2020GL088338, https://doi.org/10.1029/2020GL088338, 2020.

Graham, R. M., Cohen, L., Ritzhaupt, N., Segger, B., Graversen, R. G., Rinke, A., Walden, V. P., Granskog, M. A., and Hudson, S. R.: Evaluation of Six Atmospheric Reanalyses over Arctic Sea Ice from Winter to Early Summer, J. Climate, 32, 4121–4143, https://doi.org/10.1175/JCLI-D-18-0643.1, 2019.

Graversen, R. G., Mauritsen, T., Drijfhout, S., Tjernström, M., and Mårtensson, S.: Warm winds from the Pacific caused extensive Arctic sea-ice melt in summer 2007, Clim. Dynam., 36, 2103–2112, https://doi.org/10.1007/s00382-010-0809-z, 2011.

Guan, B. and Waliser, D. E.: Tracking atmospheric rivers globally: Spatial distributions and temporal evolution of life cycle characteristics, J. Geophys. Res., 124, 12523–12552, https://doi.org/10.1029/2019JD030536, 2019.

Guarino, M. V., Sime, L. C., Schröeder, D., Malmierca-Vallet, I., Rosenblum, E., Ringer, M., Ridley, J., Feltham, D., Bitz, C., Steig, E. J., Wolff, E., Stroeve, J., and Sellar, A.: Sea-ice-free Arctic during the Last Interglacial supports fast future loss, Nat. Clim. Change, 10, 928–932, https://doi.org/10.1038/s41558-020-0865-2, 2020.

Harrington, T. S., Zhu, J., and Skinner, C. B.: Terrestrial sources of summer arctic moisture and the implication for arctic temperature patterns, npj Clim. Atmos. Sci., 4, 25, https://doi.org/10.1038/s41612-021-00181-y, 2021.

Hegyi, B. M. and Taylor, P. C.: The unprecedented 2016–2017 Arctic sea ice growth season: The crucial role of atmospheric rivers and longwave fluxes, Geophys. Res. Lett., 45, 5204–5212, https://doi.org/10.1029/2017GL076717, 2018.

Hersbach, H., Bell, B., Berrisford, P., et al.: The ERA5 global reanalysis, Q. J. Roy. Meteor. Soc., 146, 1999–2049, https://doi.org/10.1002/qj.3803, 2020.

Hersbach, H., et al.: ERA5 hourly data on single levels from 1940 to present, Copernicus C3S CDS [data set], https://doi.org/10.24381/cds.adbb2d47, 2022a.

Hersbach, H., et al.: ERA5 hourly data on pressure levels from 1940 to present, Copernicus C3S CDS [data set], https://doi.org/10.24381/cds.bd0915c6, 2022b.

Heorton, H. D. B. S., Tsamados, M., et al.: Retrieving sea ice drag coefficients and turning angles from in situ and satellite observations using an inverse modeling framework, J. Geophys. Res.-Oceans, 124, 6388–6413, https://doi.org/10.1029/2018JC01488, 2019.

https://doi.org/10.5194/egusphere-2026-1025
Preprint. Discussion started: 20 April 2026

Hofsteenge, M. G., Graversen, R. G., Rydsaa, J. H., and Rey, Z.: The impact of atmospheric Rossby waves and cyclones on the Arctic sea ice variability, Clim. Dynam., 59, 579–594, https://doi.org/10.1007/s00382-022-06145-z, 2022.

Horvath, S., Stroeve, J., Rajagopalan, B., and Jahn, A.: Arctic sea ice melt onset favored by an atmospheric pressure pattern reminiscent of the North American-Eurasian Arctic pattern, Clim. Dynam., 57, 1771–1787, https://doi.org/10.1007/s00382-021-05776-y, 2021.

Johansson, E., Devasthale, A., Tjernström, M., Ekman, A. M. L., and L'Ecuyer, T.: Response of the lower troposphere to moisture intrusions into the Arctic, Geophys. Res. Lett., 44, 2527–2536, https://doi.org/10.1002/2017GL072687, 2017.

Komatsu, K. K., Alexeev, V. A., Repina, I. A., and Tachibana, Y.: Poleward upgliding Siberian atmospheric rivers over sea ice heat up Arctic upper air, Sci. Rep., 8, 2872, https://doi.org/10.1038/s41598-018-21159-6, 2018.

Li, L., McClean, J. L., Miller, A. J., Eisenman, I., Hendershott, M. C., and Papadopoulos, C. A.: Processes driving sea ice variability in the Bering Sea in an eddying ocean/sea ice model: mean seasonal cycle, Ocean Model., 84, 51–66, 2014a.

Li, L., Miller, A. J., McClean, J. L., Eisenman, I., and Hendershott, M. C.: Processes driving sea ice variability in the Bering Sea in an eddying ocean/sea ice model: anomalies from the mean seasonal cycle, Ocean Dynam., 64, 1693–1717, https://doi.org/10.1007/s10236-014-0769-7, 2014b.

Li, L., Cannon, F., Mazloff, M. R., and others: Impact of atmospheric rivers on Arctic sea ice variations, The Cryosphere, 18, 121–137, https://doi.org/10.5194/tc-18-121-2024, 2024.

Liang, Y., Bi, H., Huang, H., Lei, R., Liang, X., Cheng, B., and Wang, Y.: Contribution of warm and moist atmospheric flow to a record minimum July sea ice extent of the Arctic in 2020, The Cryosphere, 16, 1107–1123, https://doi.org/10.5194/tc-16-1107-2022, 2022.

Lukovich, J. V., et al.: Summer Extreme Cyclone Impacts on Arctic Sea Ice, J. Climate, 34, 4817–4834, https://doi.org/10.1175/JCLI-D-19-0925.1, 2021.

Ma, W., Chen, G., Peings, Y., and Alviz, N.: Atmospheric river response to Arctic sea ice loss in the Polar Amplification Model Intercomparison Project, Geophys. Res. Lett., 48, e2021GL094883, https://doi.org/10.1029/2021GL094883, 2021.

Mayer, M., Tietsche, S., Haimberger, L., Tsubouchi, T., Mayer, J., and Zuo, H.: An Improved Estimate of the Coupled Arctic Energy Budget, J. Climate, 32, 7915–7934, https://doi.org/10.1175/JCLI-D-18-0912.1, 2019.

Mortin, J., Svensson, G., Graversen, R. G., Kapsch, M.-L., Stroeve, J. C., and Boisvert, L. N.: Melt onset over Arctic sea ice controlled by atmospheric moisture transport, Geophys. Res. Lett., 43, 6636–6642, https://doi.org/10.1002/2016GL069330, 2016.

Nash, D., Waliser, D., Guan, B., Ye, H., and Ralph, F. M.: The role of atmospheric rivers in extratropical and polar hydroclimate, J. Geophys. Res.-Atmos., 123, 6804–6821, https://doi.org/10.1029/2017JD028130, 2018.

Notz, D. and SIMIP Community: Arctic sea ice in CMIP6, Geophys. Res. Lett., 47, e2019GL086749, https://doi.org/10.1029/2019GL086749, 2020.

Olonscheck, D., Mauritsen, T., and Notz, D.: Arctic sea-ice variability is primarily driven by atmospheric temperature fluctuations, Nat. Geosci., 12, 430–434, https://doi.org/10.1038/s41561-019-0363-1, 2019.

Overland, J. E. and Wang, M.: The 2020 Siberian heat wave, Int. J. Climatol., 41, E2341–E2346, https://doi.org/10.1002/joc.6850, 2021.

Papritz, L., Hauswirth, D., and Hartmuth, K.: Moisture origin, transport pathways, and driving processes of intense wintertime moisture transport into the Arctic, Weather Clim. Dynam., 3, 1–20, https://doi.org/10.5194/wcd-3-1-2022, 2022.

Parkinson, C. L. and Comiso, J. C.: On the 2012 record low Arctic sea ice cover: Combined impact of preconditioning and an August storm, Geophys. Res. Lett., 40, 1356–1361, https://doi.org/10.1002/grl.50349, 2013.

Peng, G., et al.: What Do Global Climate Models Tell Us about Future Arctic Sea Ice Coverage Changes?, Climate, 8, 15, https://doi.org/10.3390/cli8010015, 2020.

https://doi.org/10.5194/egusphere-2026-1025
Preprint. Discussion started: 20 April 2026

Ralph, F. M., Rutz, J. J., Cordeira, J. M., et al.: A Scale to Characterize the Strength and Impacts of Atmospheric Rivers, B. Am. Meteorol. Soc., 100, 269–289, https://doi.org/10.1175/BAMS-D-18-0023.1, 2019.

Renfrew, I. A., et al.: An evaluation of surface meteorology and fluxes over the Iceland and Greenland Seas in ERA5 reanalysis: The impact of sea ice distribution, Q. J. Roy. Meteor. Soc., https://doi.org/10.1002/qj.3941, 2020.

Simmonds, I. and Rudeva, I.: The great Arctic cyclone of August 2012, Geophys. Res. Lett., 39, L23709, https://doi.org/10.1029/2012GL054259, 2012.

Stern, D. P., et al.: The Impact of an Intense Cyclone on Short-Term Sea Ice Loss in a Fully Coupled Atmosphere-Ocean-Ice Model, Geophys. Res. Lett., 47, e2019GL085580, https://doi.org/10.1029/2019GL085580, 2020.

Tjernström, M., et al.: Warm-air advection, air mass transformation and fog causes rapid ice melt, Geophys. Res. Lett., 42, 5594–5602, https://doi.org/10.1002/2015GL064373, 2015.

Tjernström, M., Shupe, M. D., et al.: Arctic Summer Airmass Transformation, Surface Inversions, and the Surface Energy Budget, J. Climate, 32, 769–789, https://doi.org/10.1175/JCLI-D-18-0214.1, 2019.

Vázquez, M., Algarra, I., et al.: Atmospheric Rivers over the Arctic: Lagrangian Characterisation of Their Moisture Sources, Water, 11, 41, https://doi.org/10.3390/w11010041, 2019.

Wang, Z., Walsh, J., Szymborski, S., and Peng, M.: Rapid arctic sea ice loss on the synoptic time scale and related atmospheric circulation anomalies, J. Climate, 33, 1597–1617, https://doi.org/10.1175/JCLI-D-19-0215.1, 2020.

Wernli, H. and Papritz, L.: Role of polar anticyclones and midlatitude cyclones for Arctic summertime sea-ice melting, Nat. Geosci., 11, 108–113, https://doi.org/10.1038/s41561-017-0041-0, 2018.

Woods, C. and Caballero, R.: The Role of Moist Intrusions in Winter Arctic Warming and Sea Ice Decline, J. Climate, 29, 4473–4485, https://doi.org/10.1175/JCLI-D-15-0773.1, 2016.

Woods, C., Caballero, R., and Svensson, G.: Representation of Arctic Moist Intrusions in CMIP5 Models and Implications for Winter Climate Biases, J. Climate, 30, 4083–4102, https://doi.org/10.1175/JCLI-D-16-0710.1, 2017.

Zhang, J., Lindsay, R., Schweiger, A., and Steele, M.: The impact of an intense summer cyclone on 2012 Arctic sea ice retreat, Geophys. Res. Lett., 40, 720–726, https://doi.org/10.1002/grl.50190, 2013.

Zhu, Y. and Newell, R. E.: A Proposed Algorithm for Moisture Fluxes from Atmospheric Rivers, Mon. Weather Rev., 126, 725–735, 1998.